The HKU Scholars Hub   The University of Hong Kong   香港大學學術庫

Title	Origin of X-Ray and Gamma-Ray Emission from the Galactic Central Region
Author(s)	Chernyshov, D; Cheng, KS; Dogel, V; Ko, CM
Citation	The Astrophysical Journal, 2017, v. 835 n. 2, p. 194:1-11
Issued Date	2017
URL	http://hdl.handle.net/10722/240261
Rights	The Astrophysical Journal. Copyright © American Astronomical Society, co-published with Institute of Physics Publishing, Inc.; This work is licensed under a Creative Commons Attribution-NonCommercial-NoDerivatives 4.0 International License.

Origin of X-ray and gamma-ray emission from the Galactic central region

D. O. Chernyshov[1,2,3], K.-S. Cheng[2], V. A. Dogiel[1,2,4], C. M. Ko[3,5]

January 11, 2017

ABSTRACT

We study a possible connection between different non-thermal emissions from the inner few parsecs of the Galaxy. We analyze the origin of the gamma-ray source 2FGL J1745.6−2858 (or 3FGL J1745.6−2859c) in the Galactic Center (GC) and the diffuse hard X-ray component recently found by *NuSTAR*, as well as the radio emission and processes of hydrogen ionization from this area. We assume that a source in the GC injected energetic particles with power-law spectrum into the surrounding medium in the past or continues to inject until now. The energetic particles may be protons, electrons or a combination of both. These particles diffuse to the surrounding medium and interact with gas, magnetic field and background photons to produce non-thermal emissions. We study the spectral and spatial features of the hard X-ray emission and gamma-ray emission by the particles from the central source. Our goal is to examine whether the hard X-ray and gamma-ray emissions have a common origin.

Our estimations show that in the case of pure hadronic models the expected flux of hard X-ray emission is too low. Despite protons can produce a non-zero contribution in gamma-ray emission, it is unlikely that they and their secondary electrons can make a significant contribution in hard X-ray flux. In the case of pure leptonic models it is possible to reproduce both X-ray and gamma-ray emissions for both transient and continuous supply models. However, in the case of continuous supply model the ionization rate of molecular hydrogen may significantly exceed the observed value.

Subject headings: Galaxy: center - cosmic rays - gamma rays: general - X-ray: ISM

[1]I.E.Tamm Theoretical Physics Division of P.N.Lebedev Institute of Physics, Leninskii pr. 53, 119991 Moscow, Russia; `chernyshov@lpi.ru`

[2]Department of Physics, University of Hong Kong, Pokfulam Road, Hong Kong, China

[3]Institute of Astronomy, National Central University, Jhongli, Taoyuan, Taiwan, R.O.C.

[4]Moscow Institute of Physics and Technology, 141700 Moscow Region, Dolgoprudnii, Russia

[5]Department of Physics and Center for Complex Systems, National Central University, Jhongli, Taoyuan, Taiwan, R.O.C.; `cmko@astro.ncu.edu.tw`

1. Introduction

The interstellar medium of several pc around Sgr A* in the center of our Galaxy is characterized by a number of peculiar parameters (see, e.g., Ferrière et al. 2007; Ferrière 2012). The central supermassive black hole is surrounded by a circumnuclear disk (CND) whose total mass was estimated by Christopher et al. (2005) to be 10^6 $M_\odot$. The analysis of Ferrière (2012) gave a slightly lower value of mass about 2×10^5 $M_\odot$ for the region of radius $R_c = 3 \sim 5$ pc with average gas density in the CND of about 4×10^5 cm^{-3}. Unlike other regions of the Galaxy the central region shows prominent emissions in a very broad range of electromagnetic waves, from radio to gamma-ray.

- The Very Energetic Radiation Imaging Telescope Array System (VERITAS) (Archer et al. 2016) and The High Energy Stereoscopic System (H.E.S.S.) (Aharonian et al. 2009) detected a prominent gamma-ray flux in the TeV energy range. Recent observations of H.E.S.S. (Abramowski et al. 2016) with the angular resolution 0.01° provided some new information about this GC area. These observations found a point-like source in the center and a diffuse emission around the source that is correlated with the gas distribution which may mean a hadronic origin of this emission. The recovered cosmic ray density decreases as $1/r$ (where r is the distance from the source) that can be interpreted as a stationary ejection of relativistic protons by the source.

- The Large Area Telescope (*Fermi* LAT) of *Fermi* also detected a gamma-ray source in the GeV region (see Nolan et al. 2012; Acero et al. 2015). In the second *Fermi* LAT source catalog, this source was identified as the source 2FGL J1745.6−2858. The estimated gamma-ray flux from this source for $E > 2$ GeV is $I_{\rm obs} = 1.08 \times 10^{-10}$ erg cm^{-2} s^{-1} with a spectral index $\gamma = 2.68$ (see Chernyakova et al. 2011). This corresponds to a luminosity about 8×10^{35} erg s^{-1}. The positional error circle of 2FGL J1745.6−2858 overlaps with Sgr A*. This is compatible with the picture that its emission originates within the CND or within the central cavity. It is reasonable to assume that this emission is provided either by CRs protons (Chernyakova et al. 2011; Linden et al. 2012), or by CR electrons (Kusunose & Takahara 2012; Malyshev et al. 2015), or by both protons and electrons (Guo et al. 2013) produced in the vicinity of Sgr A*.

  Independent analysis of the *Fermi* LAT data by Chernyakova et al. (2011) and Malyshev et al. (2015) indicated that recovered by them spectra are compatible with 2FGL J1745.6−2858 data at GeV energies yet significantly softer in the sub-GeV range.

  In the *Fermi* LAT 4-Year Point Source Catalog (3FGL) (Acero et al. 2015), this source was identified as 3FGL J1745.6−2859c. However the gamma-ray spectrum of this source is significantly softer below 1 GeV in comparison to 2FGL J1745.6−2858. The discrepancy may be due to another bright source 3FGL J1745.3−2903c in this area, which was not identified in the second catalog. Since there is a flag "c" in the name of the source the reliability of the derived spectrum of 3FGL J1745.6−2859c is not very high due to the contamination from the nearby bright source. In this paper we do not judge which analysis is more appropriate, instead we present our model fittings for both 3FGL data and data obtained by Malyshev et al. (2015).

- Large scale diffuse radio emission from this region is known as radio halo. It has a spherical shape with radius of about 8 pc. At frequencies about tens of GHz the emission have a clear synchrotron nature and thus confirms the presence of high-energy electrons in this area (Pedlar et al. 1989).

- The Nuclear Spectroscopic Telescope Array (*NuSTAR*) found a flux of non-thermal hard X-ray emission in the direction of the central few parsecs region of the Galaxy (Perez et al. 2015). Total luminosity in the energy range 20-40 keV was estimated as 2.4×10^{34} erg s^{-1}, which corresponds to an energy flux at the Earth of 3.3×10^{-12} erg cm^{-2} s^{-1}. Spatial profile of the emission has an elliptical shape with a major axis 8 pc and a minor axis 4 pc. It is larger than gas structures in the GC like the central cavity (1.2 pc in diameter) and CND (6 pc in diameter) (Ferrière 2012). It also does not spatially coincide with Sgr A East. However it looks similar to the Nuclear Star Cluster (8 pc by 5.6 pc, Schödel et al. 2014). Therefore it was concluded that this emission was produced by unresolved point like sources. This idea was further developed by Hailey et al. (2016) who concluded that the X-ray emission can be produced by intermediate polars (a type of cataclysmic variables) with masses of about 0.9 solar masses.

Despite the fact that point-like sources potentially play a major role in the hard X-ray emission we suppose that there is still room for a diffuse component of X-rays generated by CRs. Indeed as we mentioned earlier the presence of high-energy protons or electrons is confirmed by gamma-ray and radio observations. It is perceivable that these energetic particles also contribute to the total hard X-ray flux from the GC.

In principle, hard X-ray photons may be generated by synchrotron emission of secondary high-energy electrons produced by collisions of TeV protons with the background gas in the GC region. Recent observations of TeV gamma-ray point-like source detected a clear cut-off in the gamma-ray spectrum (Archer et al. 2016) at around 12 TeV. This gives the maximum energy of primary protons at about $12/0.075 = 160$ TeV. The maximum energy of secondary electrons is thus about $12 \times 0.039/0.075 = 6.24$ TeV (see Atoyan 1992). Therefore, in order to produce a non-thermal emission with power-law spectrum up to 40 keV by secondary electrons, the magnetic field strength there should be about 16 mG. This value is significantly higher than the $1 \sim 3$ mG obtained by Killeen et al. (1992); Yusef-Zadeh et al. (1996); Eatough et al. (2013). Hence we must conclude that synchrotron origin of this X-rays is doubtful.

If however the cut-off in the spectrum of this source is due to absorption of the gamma-ray photons by their interactions with background infra-red emission as suggested by Abramowski et al. (2016), the spectrum of primary protons may be power-law up to energies higher than 140 TeV. In this case synchrotron emission can produce up to 10%-20% of the flux detected by *NuSTAR* depending on the magnetic field strength. We note however that the density of the infra-red photons does not appear to be high enough to produce the observed cut-off in the gamma-ray spectrum by photon-photon ($\gamma\gamma$) collisions (see, e.g., Kistler 2015).

Alternatively, X-rays can be generated by electron bremsstrahlung or inverse Compton ef-

fect (or both). This model was developed in Chernyshov et al. (2014). They assumed that the gamma-ray flux of the source 2FGL J1745.6−2858 is generated by relativistic protons in CND. The secondary electrons produce a flux of hard X-rays by bremsstrahlung in CND and by inverse Compton effect in the region surrounding CND. Then the X-ray halo around CND could be more extended than the gas distribution as observed by *NuSTAR*. However, Chernyshov et al. (2014) considered a spherically symmetric model which is unable to explain the observed asymmetry of the hard X-ray emission. Besides, the hard X-ray flux predicted in that work turned out to be significantly lower than the observed value. Therefore, modification of the model is required if this interpretation is correct.

Thus, these observations indicate a high efficiency CR production in the GC. Additional evidence supporting high density of CRs in the GC came from the measured ionization rate in the 1 pc region of CND by Goto et al. (2013, 2014). They obtained a value $\zeta \simeq 1.2 \times 10^{-15}$ s^{-1}, which is one order of magnitude higher than in other parts of the Galaxy. This ionization is most likely produced by subrelativistic CRs with a density higher than those outside the GC region. The estimated source luminosity of these subrelativistic CRs in the GC is about $10^{38} \sim 10^{39}$ erg s^{-1} (see, e.g., Dogiel et al. 2013, 2014; Yusef-Zadeh et al. 2013).

The goal of our present investigation is to explain simultaneously all phenomena mentioned above except TeV gamma-ray emission in the framework of a single model where CRs are injected from the central source. This source may be stationary (Macias et al. 2015; Abramowski et al. 2016) or transient (Macias et al. 2015). Both possibilities will be discussed. We will estimate the required parameters of this source.

We analyze two types of models of the source:

- *Hadronic model.* The central source injects mainly high energy protons. Most of the non-thermal electrons is produced by interactions of these protons with background medium. Gamma-rays are generated by proton-proton (pp) collisions. X-rays are produced by protons via inverse bremsstrahlung and by secondary electrons through bremsstrahlung and inverse Compton scattering. Radio emission is produced by synchrotron losses of secondary electrons.

- *Leptonic model.* The central source injects primary high energy electrons. In this case gamma-ray and hard X-ray emission are mainly produced by their bremsstrahlung and inverse Compton scattering. Radio flux is produced by their synchrotron emission.

Unlike previous investigations our goal is to explain all types of non-thermal emissions using the same injection of particles (protons or electrons). The ultimate goal is to reproduce the observed hard X-ray spectrum and the spatial distribution of hard X-rays using the observed gamma-ray spectrum as a reference point to determine the injection and propagation parameters. Also we examine whether the estimated gamma-ray flux in the models is compatible with other observations there, such as the radio emission and the ionization rate of molecular hydrogen. Below we take into

account the non-spherical shape of the gas distribution in the central few parsecs. The parameters of the gas distribution in the CND region are taken from Ferrière (2012).

In this investigation we assume that TeV gamma-ray emission discovered by H.E.S.S. and VERITAS, and GeV gamma-ray emission discovered by *Fermi* LAT are produced by two different sources. Indeed the overall gamma-ray spectrum indicates an "ankle-like" break at the transition from GeV to TeV energies. This break can be described naturally by a combination of two components with different spectral indices. Since TeV component exhibits much harder spectrum, its contribution to X-rays, radio emission and ionization should be much lower in comparison to GeV component. Therefore we restrict our analysis to GeV gamma-rays only.

2.   Model description

We use a cylindrically symmetric model to study the evolution of proton and electron distribution functions $f_p(t, r, z, E)$ and $f_e(t, r, z, E)$ with time. The $z = 0$ plane corresponds to the CND plane of symmetry, and the origin $(r, z) = (0, 0)$ corresponds to the center of the CND with Sgr A* as the source. Equation for the distribution functions is

$$\frac{\partial f_{p,e}}{\partial t} - \frac{\partial}{\partial z}\left(D_{p,e}\frac{\partial f_{p,e}}{\partial z}\right) - \frac{1}{r}\frac{\partial}{\partial r}\left(rD_{p,e}\frac{\partial f_{p,e}}{\partial r}\right) + \frac{\partial}{\partial E}\left[\left(\frac{dE}{dt}\right)_{p,e}f_{p,e}\right] = Q_{p,e}(t, r, z, E). \qquad (1)$$

Here we assume that the diffusion is isotropic and the diffusion coefficient $D_{p,e} = D_{p,e}(E, r, z)$ has different values inside and outside the molecular cloud. The diffusion coefficient is a function of particle rigidity,

$$D_{p,e}(E, r, z) = D_0(r, z)\beta\left(\frac{p}{p_0}\right)^\varsigma, \qquad (2)$$

where the value of D_0 is the same for protons and electrons, p is the particle momentum, β is the particle velocity in the units of c, $p_0 = 4$ GeV/c, and the spectral index ς is determined by the spectrum of MHD-turbulence for non-magnetized particles or by a structure of magnetic field lines for magnetized particles. Outside the cloud we assume that the diffusion is mainly due to energetic particle scattering by the interstellar turbulence with Kolmogorov spectrum and therefore $\varsigma^{\mathrm{inter}} = 0.33$ (Ackermann et al. 2012).

Inside the molecular cloud, however, the situation is quite different due to the very efficient damping of MHD waves by ion-neutral friction. In this case diffusion is due to tangled magnetic field. Therefore the mean-free path of charged particles is determined by the characteristic correlation length of the intracloud magnetic field. As a result the diffusion coefficient does not depend on particle rigidity and $\varsigma^{\mathrm{cloud}} = 0$ (see, e.g., Dogiel et al. 2015).

The parameter D_0 in the GC center region and inside the CND is unknown. For some regions of the Galaxy, it can be estimated from observational data. Ackermann et al. (2012) gave a value

of $D_0^{\mathrm{inter}} = 5 \sim 10 \times 10^{28}$ cm^2 s^{-1} as an average over the Galaxy diffusion coefficient. As for intracloud, diffusion estimations for cloud such as Sgr B2 gave a value of about $D_0^{\mathrm{cloud}} = 10^{28}$ cm^2 s^{-1} (Dogiel et al. 2015).

However, the inner few parsec of the Galaxy are located in a special region characterized by processes of effective energy release in different forms. Therefore, it is reasonable to assume that the diffusion coefficient there is significantly smaller than in the other part of the GC region. We estimate this parameter from the spatial and spectral properties of the emissions.

The energy loss term dE/dt in Equation (1) consist of Coulomb losses and proton-proton losses for protons (Mannheim & Schlickeiser 1994), and of Coulomb, bremsstrahlung, inverse-Compton and synchrotron losses for electrons (Blumenthal & Gould 1970). The source term $Q_{p,e}(t, r, z, E)$ are model-dependent and we derive them later (see sections 3 and 4).

We adopt the ambient density distribution from Ferrière (2012). We divide the space into the following regions: (1) central cavity with density of 10^3 cm^{-3}, (2) outer layer of CND with density of 3.2×10^4 cm^{-3}, (3) CND with density of 4.4×10^5 cm^{-3}, and (4) radio halo with density of 210 cm^{-3} (see Figure 1).
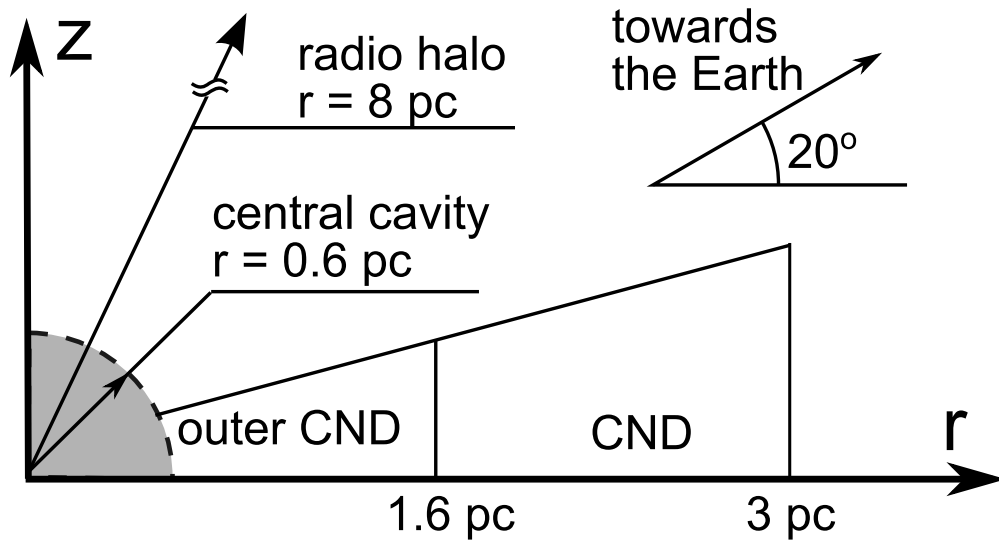

Fig. 1.— Gaseous structure in the Galactic Center region (Ferrière 2012).

In order to estimate the electron energy loss and their emission we need to know the distribution of soft photons. We take into account the following components (assuming they all have black-body spectrum): (1) optical emission from the central cluster ($T = 3 \times 10^4$ K), (2) mid-infrared emission from the central cluster ($T = 170$ K), (3) dust emission from CND ($T = 70$ K), and (4) optical emission from the nuclear star cluster ($T = 3500$ K). Details on the estimation of soft photon density can be found in Appendix A.

From equation (1) we derive the evolution of the distribution functions f_p and f_e and the gamma-ray emission produced by these CRs

$$I_\gamma(t, E_\gamma) = \int dV \quad \left[\int dE \ f_p(t, r, z, E) n(r, z) v \left(\frac{d\sigma(E, E_\gamma)}{dE_\gamma} \right)_{pp} \right.$$
$$+ \int dE \ f_e(t, r, z, E) w(r, z) v \left(\frac{d\sigma(E, E_\gamma)}{dE_\gamma} \right)_{\mathrm{IC}}$$
$$\left. + \int dE \ f_e(t, r, z, E) n(r, z) v \left(\frac{d\sigma(E, E_\gamma)}{dE_\gamma} \right)_{\mathrm{br}} \right] , \qquad (3)$$

where v is particles velocity, $n(r, z)$ and $w(r, z)$ are the density distributions of ambient gas and soft photons, respectively. Proton-proton cross-section $(d\sigma/dE_\gamma)_{pp}$ is taken from Kamae et al. (2006), bremsstrahlung $(d\sigma/dE_\gamma)_{\mathrm{br}}$ and inverse-Compton cross-sections $(d\sigma/dE_\gamma)_{\mathrm{IC}}$ are taken from Blumenthal & Gould (1970).

We adjust the initial parameters to make sure that gamma-ray spectrum $I_\gamma(E_\gamma)$ matches the observed one by *Fermi* LAT. With these parameters X-ray emissivity can be estimated as

$$\epsilon(t, r, z, E_x) = \quad \int dE \ f_p(t, r, z, E) n(r, z) v \left(\frac{d\sigma(E, E_x)}{dE_x} \right)_{\mathrm{ib}}$$
$$+ \int dE \ f_e(t, r, z, E) w(r, z) v \left(\frac{d\sigma(E, E_x)}{dE_x} \right)_{\mathrm{IC}}$$
$$+ \int dE \ f_e(t, r, z, E) n(r, z) v \left(\frac{d\sigma(E, E_x)}{dE_x} \right)_{\mathrm{br}} , \qquad (4)$$

where $(d\sigma(E, E_x)/dE_x)_{\mathrm{ib}}$ is the cross-section of the inverse-bremsstrahlung process (Hayakawa 1964; Tatischeff 2003).

To obtain the spatial distribution of X-rays across the sky, the emissivity should be integrated along the line-of-sight. We take into account the fact that CND is inclined to the Galactic plane by $20°$ (see Figure 1).

Ionization rate of molecular hydrogen is computed from

$$\zeta = \int dE \ \sigma_{Hp} v f_p + \int dE \ \sigma_{He} v f_e , \qquad (5)$$

where σ_{Hp} and σ_{He} are the cross-sections of hydrogen ionization by proton and electron impact, respectively (Tatischeff 2003). We combine Equation (5) with the approach of Dalgarno et al. (1999) to take into account of the influence low-energy electrons.

Equations (3), (4) and (5) are applicable to both hadronic and leptonic models. Obviously, in the case of leptonic model we assume $f_p \equiv 0$ and ignore all terms related to protons.

3. Hadronic models

We start from injection spectrum of primary protons. Energetic electrons are considered as secondaries and their source function is

$$Q_e(t,r,z,E) = n(r,z) \int dE_p f_p(t,r,z,E_p) v \left(\frac{d\sigma(E_p,E)}{dE} \right)_{\text{se}}, \qquad (6)$$

where the cross-section $(d\sigma/dE)_{\text{se}}$ of electron production includes proton-proton collision term (Kamae et al. 2006) and the knock-on term (Hayakawa 1964).

The source function of protons is model-dependent. We adopt the following form,

$$Q_p(t,r,z,E) = A(E) \, T(t) \, \delta(z) \, \frac{\delta(r)}{2\pi r}, \qquad (7)$$

where $\delta(z)$ and $\delta(r)$ are Dirac delta-functions of z and r, respectively. $A(E)$ is the spectrum of the injected particles and $T(t)$ describes the temporal variations of the injection.

The injected particle spectrum is assumed to be a power-law in momentum space, i.e.,

$$\frac{dN(>p)}{dp} \propto p^{-\alpha}, \qquad (8)$$

where p is the momentum of the particle, α is a spectral index of of the injection spectrum and $N(>p)$ is total number of particles with momenta higher than p. One should note that a momentum power-law distribution of particles is expected inside of accelerator while the injected spectrum of particles may be modified by energy losses or escape which will potentially develop a spectral break. This is really important since we perform calculations in a wide energy range - from non-relativistic to ultra-relativistic energies. However in the particular case of the hadronic model we would like to maximize potential X-ray emission so we assume that particles are injected with power-law spectrum without any breaks.

After re-expressing Equation (8) in terms of kinetic energy E, we obtain the spectrum $A(E)$ in Equation (7)

$$A(E) = A_0 \, (E + Mc^2) \, (E^2 + 2Mc^2 E)^{-(\alpha+1)/2}, \qquad (9)$$

where E and M are the kinetic energy and mass of the particle, respectively. In the present section we take $M = m_p$, the mass of proton.

The normalization constant A_0 and the spectral index α of Equation (9) can be estimated from the gamma-ray data. Their values should be adjusted to fit the observed gamma-ray spectrum. With these parameters one can estimate the intensity of hard X-rays and radio emission.

Radio emission depends strongly on the magnetic field strength whose value has not been well established. Hence radio emission cannot be considered as a strong indicator for the validity of the model. The same is true for the ionization rate whose value is known only up to an order of magnitude. Therefore, we consider that these two observations play a supplementary role in our discussion, and we mainly concentrate on hard X-ray emission to examine whether the model is compatible with observations or not.

3.1.   Single-burst hadronic model

In the framework of this model, we assume that the injection happened some time ago in the form of a short burst. The temporal term of the injection function in Equation (7) is expressed as $T(t) = \delta(t)$.

The observed spectrum of Malyshev et al. (2015) can be reproduced by assuming $\alpha = 2.5$ in Equation (9), and $\alpha = 2.3$ for the 3FGL data (Acero et al. 2015) (see the left panel of Figure 2). As one can see from the figure the fit of the data is not very good. It was indicated by Malyshev et al. (2015) that the low-energy part of the spectrum cannot be explained in the framework of pure hadronic model, and the situation is worse in the case of 3FGL data.

Gamma-ray spectrum depends weakly on time t and the diffusion coefficients. However the intensity of hard X-ray emission is more sensitive to these parameters. Its value increases as the diffusion coefficients decrease. To maximize the intensity of X-rays we used the following propagation parameters: inside the cloud $D_0^{\text{cloud}} = 10^{26}$ cm^2 s^{-1} while outside the cloud $D_0^{\text{inter}} = 10^{27}$ cm^2 s^{-1} (see Equation 2). The evolution of the hard X-ray intensity with time is presented in the right panel of Figure 2.
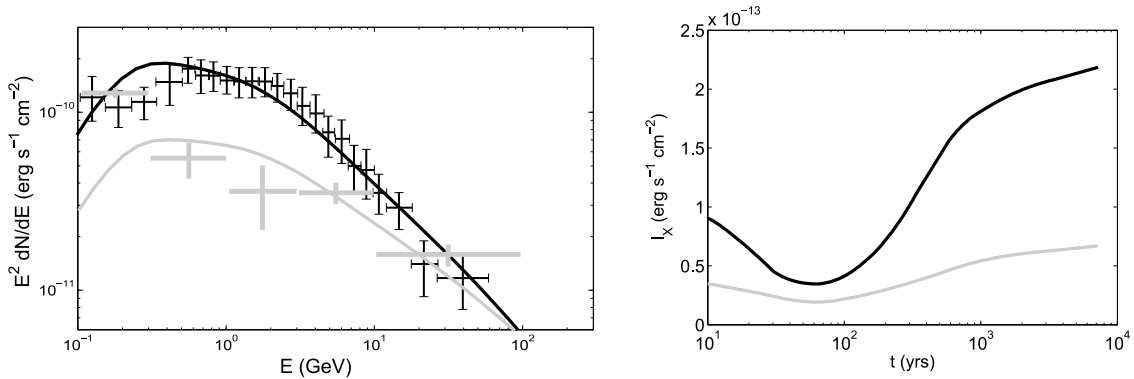

Fig. 2.— *Left:* Gamma-ray spectrum in the case of single-burst hadronic model. Black crosses with tick mark are data points taken from Malyshev et al. (2015) and gray crosses from 3FGL (Acero et al. 2015). *Right:* Evolution of the hard X-ray intensity in the case of single-burst hadronic model. In both panels, theoretical curves corresponding to Malyshev et al. (2015) and 3FGL (Acero et al. 2015) are black and gray, respectively.

The resulting X-ray intensity in the model is significantly less than the value of 3.3×10^{-12} erg cm^{-2} s^{-2} observed by *NuSTAR*. This conclusion agrees with Chernyshov et al. (2014). Although the curves in right panel of Figure 2 show a tendency to increase with time, an unreasonably long time and unreasonably high energy of the initial burst are needed to reach the observed value. Therefore, we conclude that single-burst hadronic model is unable to reproduce the observed hard X-ray emission from the GC. However, relativistic protons may produce a non-negligible contribution
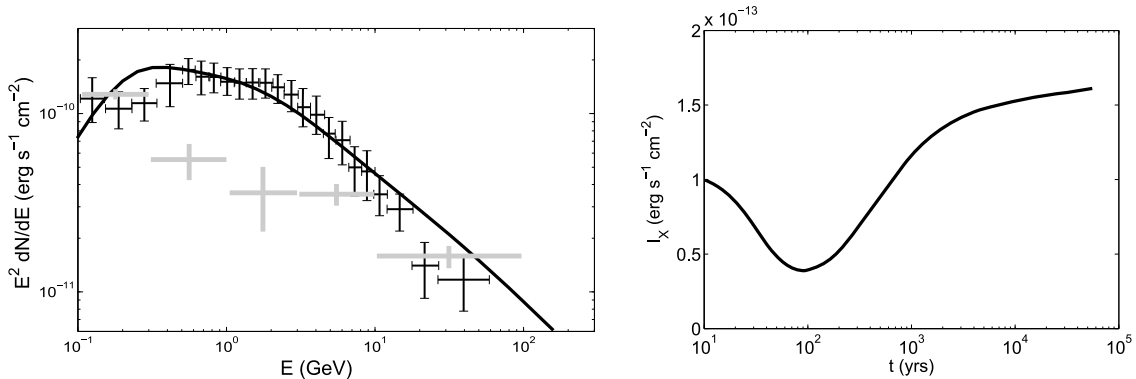
Fig. 3.— The same as Figure 2 except for the case of continuous supply hadronic model.

to the gamma-ray emission.

The total energy budget to produce gamma-ray emission depends on how long ago the injection of protons took place. Since protons escape from the region with dense gas, the longer the time from the injection, the higher the energy is required. For characteristic time about $2000 \sim 7000$ yrs, the total energy required is within $(0.15 \sim 1) \times 10^{50}$ erg. One can see that a single supernova explosion can supply enough energy assuming 10% acceleration efficiency.

3.2. Continuous supply hadronic model

In this case the temporal term of the injection function in Equation (7) is expressed as $T(t) = \Theta(t)$, where $\Theta(t)$ is the Heaviside step function.

The results are shown in Figure 3. The total power required is about 5×10^{37} erg/s. Both gamma-ray and X-ray results do not differ strongly from that of the single-burst hadronic model except that the X-ray emission is even lower. Therefore, the conclusion is not in favor of continuous supply (or stationary) model also.

4. Leptonic models

In this section we assume that the central source injects relativistic electrons. The source function of electrons in Equation (1) is similar to that used in Section 3 (see Equation (7)),

$$Q_e(t, r, z, E) = A(E) \, \Theta(E_{\max} - E) \, T(t) \, \delta(z) \, \frac{\delta(r)}{2\pi r} \,, \tag{10}$$

where the energy part $A(E)$ is described by Equation (9) with $M = m_e$, the electron mass. We introduced a cut-off energy $E_{\max}$ (the Heaviside step-function in Equation (10)) to reproduce a

turn-over in the gamma-ray spectrum at 2 GeV. We note that this cut-off can occur when the electrons pass through a region with very high magnetic or radiation field before they escape into the interstellar medium (Malyshev et al. 2015).

Similar to hadronic scenario we would like to maximize potential X-ray emission, we assume that particles are injected with power-law spectrum without any breaks. However it is necessary to mention that spectrum of electrons below 100 MeV is heavily influenced by ionization losses and therefore is weakly sensitive to the spectral index of the injected spectrum. We estimate the potential impact of a break in the injected spectrum of electrons below.

Taking all these changes into account we repeat the same procedures in Section 3.

4.1. Single-burst leptonic model

Similar to Section 3.1, the temporal term of the injection function in Equation (10) is expressed as $T(t) = \delta(t)$.

For the observed gamma-ray spectrum of (Malyshev et al. 2015), in order to reproduce the cut-off in the data at about 2 GeV, we take two sets of value of spectral index and cut-off energy, (i) $\alpha = 2.1$ with $E_{\max} = 50$ GeV, and (ii) $\alpha = 2.3$ with $E_{\max} = 100$ GeV. For 3FGL data, we take $\alpha = 2.5$, and choose $E_{\max} \to \infty$ (or simply neglect the Heaviside step-function in Equation (10)) because there is no spectral break in 3FGL data and the high energy cut-off is not necessary.

In the case of leptonic models, X-ray and gamma-ray emission consists of bremsstrahlung and inverse-Compton components. The energy losses through inverse-Compton effect produces a softer spectrum in X-rays than by bremsstrahlung. Therefore, for the same intensity of gamma-ray emission one would expect higher intensity of X-rays if inverse-Compton effect dominates.

Thus, in order to maximize the intensity of X-rays (with a given gamma-ray intensity), it is necessary to reduce the bremsstrahlung component of the emission as much as possible. To achieve this effect, we adjust values of the diffusion coefficients. Similar to the case of hadronic model we choose fairly low value of diffusion coefficients inside the cloud $D_0^{\text{cloud}} = 10^{26}$ cm^2 s^{-1} (see Equation 2). Outside the cloud, however, we use a much larger value of the diffusion coefficient $D_0^{\text{inter}} = 10^{28}$ cm^2 s^{-1} to prevent the particles propagating back to the cloud.

Spatial distribution of hard X-ray emission is time-dependent. To reproduce the observed spatial profile of X-rays with the assumed diffusion coefficients, it is necessary to allow at least 7×10^2 years has passed after the injection.

Gamma-ray spectra produced in leptonic models are shown in the left panel of Figure 4. The black dashed line is the case of $\alpha = 2.1$ and black solid line is the case of $\alpha = 2.3$. The gray line corresponds to $\alpha = 2.5$ in 3FGL data. We present the solution at $t = 7 \times 10^2$ years. One can see that the gamma-ray emission is reproduced quite well in the case of $\delta = 2.1$ but for the case of
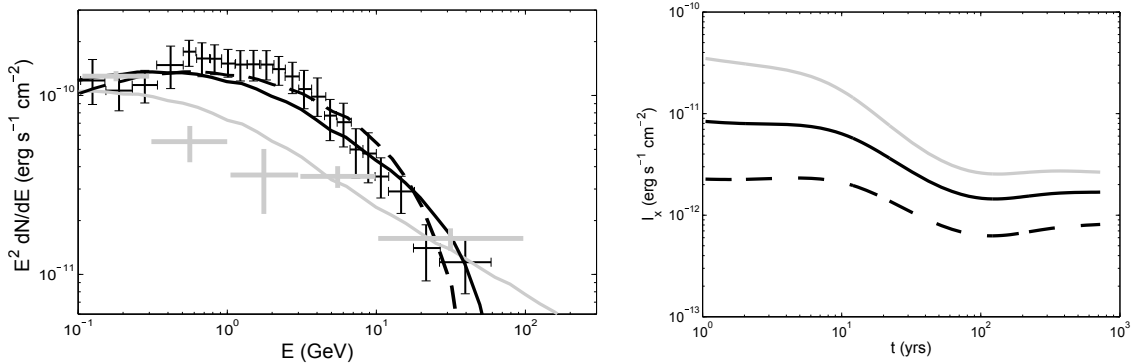
Fig. 4.— The same as Figure 2 except for the case of single-burst leptonic models. Black solid lines correspond to $\alpha = 2.3$ and dashed lines to $\alpha = 2.1$. Gray lines are based on 3FGL data with $\alpha = 2.5$.

$\delta = 2.3$ there is a deficit around a few GeV.

The evolution of the intensity of hard X-rays is shown in the right panel of Figure 4. Once again, the black dashed line is the case of $\alpha = 2.1$ and black solid line is the case of $\alpha = 2.3$, and the gray line corresponds to $\alpha = 2.5$ in 3FGL data. One can see that if the spectrum of electrons is harder (smaller α), the intensity of hard X-ray emission is lower. In all cases, the intensity of hard X-rays (at $t \sim 10^3$ years) is within a factor of two around the value 3.3×10^{-12} erg cm^2 s^{-1} observed by $NuSTAR$. Since the uncertainty of the X-ray flux is high, this can be considered as a good fit.

To estimate the potential effect of a spectral break in the injected spectrum of electrons we introduced a low-energy cut-off and recalculated the intensity of hard X-ray emission. We took injection spectrum with index of $\alpha = 2.5$ as it should be the most significantly affected one. Positions of the cut-off were chosen to be at $E_{min} = 1$ MeV, 10 MeV, 30 MeV and 100 MeV. Gamma-ray data do not allow us to place a cut-off above 100 MeV. The corresponding hard X-ray flux in these cases are 1.0, 0.7, 0.4 and 0.2 of the original value. In more realistic scenarios with a spectral break instead of a low-energy cut-off the expected drop of the X-ray emission should be lower. Therefore we consider a single power-law spectrum is a reasonable assumption taking into account that actual X-ray emission may be reduced by a factor of few.

Different components of the emission contributing to X-rays and gamma-rays are presented in Figure 5. One can see that emission is clearly dominated by bremsstrahlung process. Therefore, the intensity of hard X-ray emission may be higher if we underestimated the ratio between soft photons and gas in the central few parsecs.

Spatial profile of the hard X-ray emission is also reproduced quite nicely (see Figure 6). To compare the $NuSTAR$ data taken from Perez et al. (2015), we multiply the computed X-ray flux by some number to match the data and added a constant background flux of the order of 10^{-5}
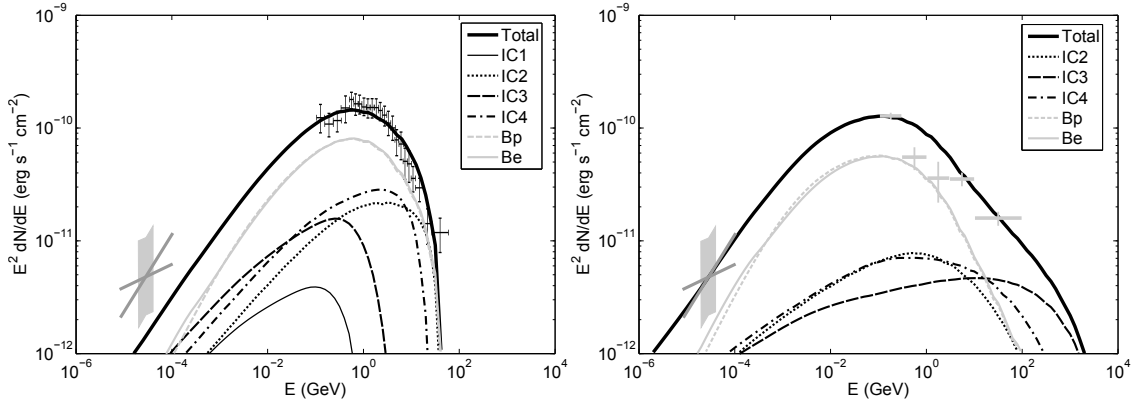
Fig. 5.— Spectrum of different components of the emission expected in leptonic models. Here IC1 corresponds to inverse-Compton scattering on IR photons produced by CND, IC2 - on UV photons produced in the central parsec, IC3 - on IR photons produced in the central parsec, and IC4 - on visible photons produced by NSC; Bp corresponds to electron-ion bremsstrahlung and Be - to electron-electron bremsstrahlung. Black crosses represent data from Malyshev et al. (2015) and gray crosses data from 3FGL. Gray area shows the hard X-ray flux observed by *NuSTAR* with X-shaped mark demonstrating the allowed minimum and maximum spectral indices. *Left:* Injection index is $\alpha = 2.1$. *Right:* Injection index is $\alpha = 2.5$ (for 3FGL data).

counts s^{-1} $arcsec^{-1}$. Excess emission observed at the position of Sgr A* may be due to X-ray filament G359.97−0.038.

The total energy budget required to produce observed gamma-ray emission depends on how long ago the injection took place (see the left panel of Figure 7). Since electrons are affected by energy losses and escape process, it is natural that the required energy increases as the time from the injection increases. One can see that the overall energy is quite high. However in all cases, injection can be produced by a single supernova explosion with electron acceleration efficiency of about 10%.

In the right panel of Figure 7, we show the evolution of ionization rate of molecular hydrogen estimated in two locations, (1) in the central cavity, and (2) averaged over CND. One can see that in both cases at $t = 7 \times 10^2$ years the estimated values do not contradict the measured value $\zeta \simeq 1.2 \times 10^{-15}$ s^{-1} (Goto et al. 2013, 2014). Shape of the injected spectrum at low energies have higher impact on the ionization rate in comparison to the impact on the X-ray flux. For spectra with cut-off at $E_{min} = 1$ MeV, 10 MeV, 30 MeV and 100 MeV, the value of ionization rate in the central cavity becomes 1.0, 0.45, 0.12, 0.03 of the original value. The corresponding values of ionization rate averaged over CND are 1.0, 0.75, 0.4, 0.16 of the original value and they are very close to the corresponding modifications of the X-ray flux. Therefore ionization rate in the central cavity can be slightly reduced by an adjustment of the spectral shape. On the other hand the value
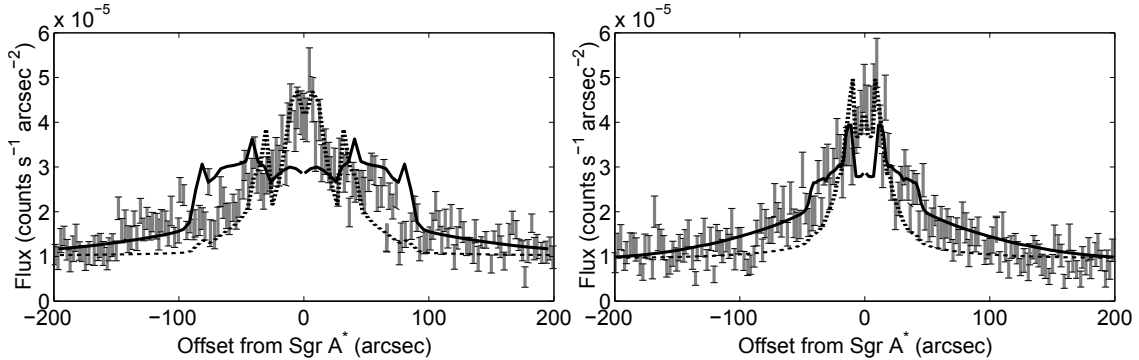
Fig. 6.— Spatial profile of the hard X-ray emission along the Galactic longitude (on the left) and latitude (on the right) in the case of leptonic models. Solid curves correspond to single-burst model at $t = 700$ years and dotted curves to continuous supply model. Data are taken from Perez et al. (2015).

of ionization rate averaged over CND is tied to the intensity of the hard X-rays and there are not much freedom. In any case, as we mentioned before the measured ionization rate is uncertain up to an order of magnitude in values and cannot be considered as a very reliable restriction.

Another important indicator related to ionization is the intensity of 6.4 keV Kα line of neutral iron. For solar abundance of iron we obtained the following intensities of the emission from CND, (1) for $\alpha = 2.1$ we expect $I_{6.4} = 1.3 \times 10^{-7}$ ph cm^2 s^{-1}, (2) for $\alpha = 2.3$ we expect $I_{6.4} = 2.3 \times 10^{-7}$ ph cm^2 s^{-1}, and (3) for $\alpha = 2.5$ we expect $I_{6.4} = 2.8 \times 10^{-7}$ ph cm^2 s^{-1}. It is worth noting that if we consider the whole region of interest, then the expected equivalent width of this line will be about 15 eV. This value is extremely low since only a small part of X-ray emission comes from the molecular gas. Moreover, since this region is also contaminated by thermal emission from Sgr A East which we did not take into account. One can expect even lower values of the equivalent width of this line.

The expected radio emission from radio halo is shown in Figure 8. Experimental data were taken from Pedlar et al. (1989). To match the data-points, we assumed that the average magnetic field is of the order of $H = 44$ μG in the case of $\alpha = 2.1 \sim 2.3$, and $H = 54$ μG in the case of $\alpha = 2.5$. We also take into account of free-free absorption by the plasma of radio halo. One can see that the data point at low frequency is fitted poorly, but we can assume that there is an additional thermal component of radio emission as assumed by Pedlar et al. (1989).

4.2. Continuous supply leptonic model

This model assumes that central source supplies energetic electrons continuously. The temporal term of the injection function in Equation (10) is expressed as $T(t) = \Theta(t)$. For the energy part
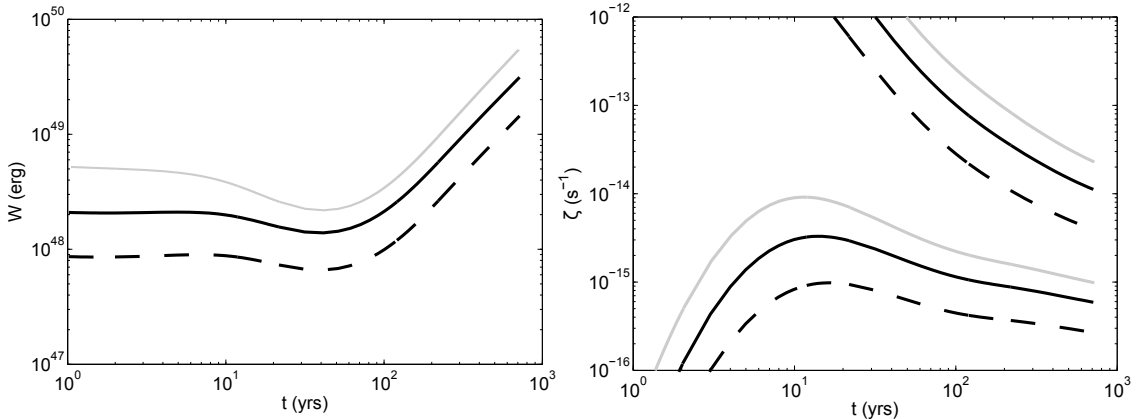
Fig. 7.— *Left:* Total energy of injected electrons required to reproduce observed gamma-ray emission in the case of single-burst leptonic model depending on how long ago the injection of the particles took place. Black solid line is the case of injection index $\alpha = 2.3$, black dashed line is $\alpha = 2.1$, and gray line is $\alpha = 2.5$. *Right:* Ionization rate in the case of single-burst leptonic model. Top curves - in the central cavity, bottom curves - averaged over CND. Other notations are the same.

we assume that the spectral index is $\alpha = 2.5$ and the cut-off energy is $E_{\max} = \infty$.

Gamma-ray emission and evolution of hard X-ray flux from the model looks promising as shown in Figure 9. The spatial distribution of X-ray emission is slightly narrower than the one observed by NuSTAR, see dotted line in Figure 6. Nevertheless, it is still consistent with the observational data. Total energy required to reproduce the data is about 4.6×10^{38} erg s^{-1}. The only problem of the continuous supply model is that the ionization rate ζ in the central cavity exceeds 10^{-11} s^{-1} which is more than 4 orders of magnitude higher than reported by Goto et al. (2014). On the other hand, average ionization rate inside the CND is about 3×10^{-15} s^{-1} and does not differ significantly from the experimental value.

The reason for the very high ionization rate in the central area originate from the characteristic of the source of particles there. Indeed, stationary solution gives a $1/r$ distribution near the center, which produces a huge spike of particle density in the central region. Now suppose we turn off the source and wait for about 100 years, the particles will spread out and the ionization rate will drop significantly to a more reasonable value of about $\zeta \simeq 5 \times 10^{-14}$ s^{-1}.

Another way to reduce the ionization rate is to assume that injected spectrum has a spectral break at low energies. Despite the fact that such modification does not affect the average particle distribution at large distances where it is modified by energy losses the low-energy spectral shape may be important near the source. This assumption may decrease the expected ionization rate near the center even further.
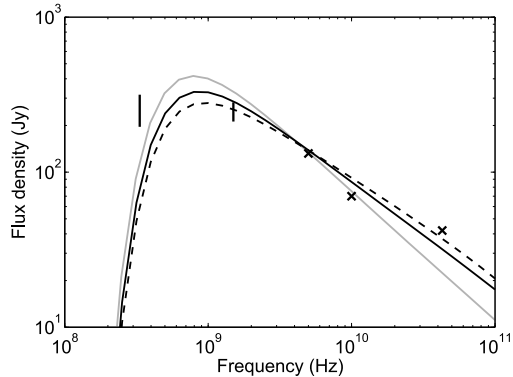
Fig. 8.— Spectrum of the radio emission from the radio halo in the case of single-burst leptonic model. Black solid line is the case of injection index $\alpha = 2.3$, black dashed line is $\alpha = 2.1$, and gray line is $\alpha = 2.5$. Data are taken from Pedlar et al. (1989).
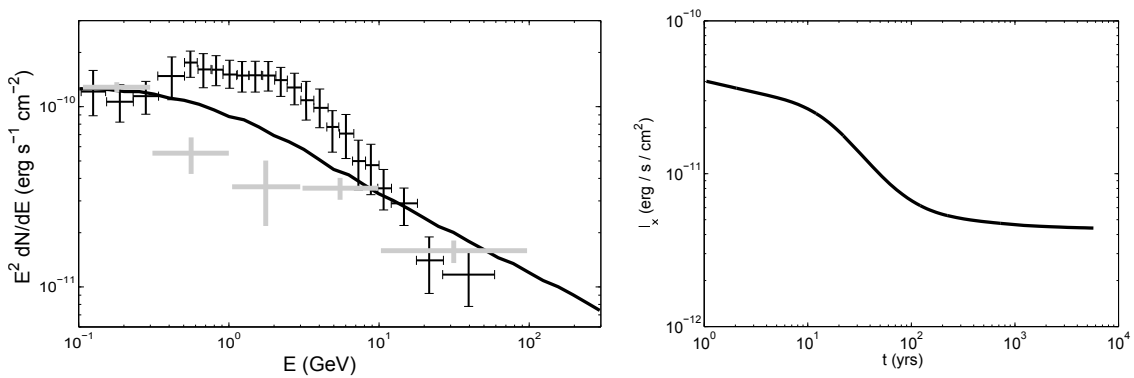

Fig. 9.— The same as Figure 2 except for the case of continuous supply leptonic model.

5. Mixed models

It is more common and conceivable that both primary electrons and protons are accelerated in the same astrophysical source. For example, the observed composition of cosmic rays in the vicinity of the Earth suggests that potential sources of cosmic rays produce protons and electrons above 1 GeV in a ratio from 100:1 to 50:1 (Strong et al. 2010). To take this possibility into account, we made a linear combination of hadronic and leptonic models. We assumed that both primary protons and primary electron have the same injection spectral index $\alpha = 2.5$. The resulting spectrum is shown in Figure 10. One can see that for near Earth proton-to-electron ratio (100 : 1) the hard X-ray flux is too low because the emission is dominated by the hadronic component. However, if we reduce the proton-to-electron ratio to 30:1, charged particles can make a non-negligible contribution to the hard X-ray flux.

It is worth noting that proton-to-electron ratio deduced here is much higher than the one deduced from direct comparison of energy budgets from Sections 3 and 4. The reason for this discrepancy is that here we use propagation parameters from Section 4 for both hadronic and leptonic components. These parameters significantly reduce gamma-ray emission from protons in comparison with those from Section 3. Therefore proton-to-electron ratio becomes higher.
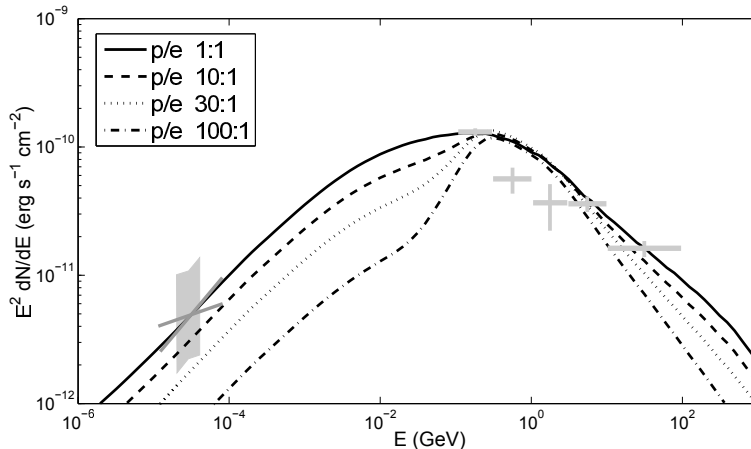

Fig. 10.— Multi-wavelength spectrum of the emission expected in the mixed models for different proton-to-electron density ratio above 1 GeV. The injection particles spectral index is $\alpha = 2.5$. Gray crosses represent gamma-ray data from 3FGL (Acero et al. 2015). Gray area represent data from *NuSTAR* and the X-shaped mark shows the allowed minimum and maximum spectral indices.

6. Conclusions

We analyzed the propagation of the charged particles emitted by a central source in the GC and their interactions with the surrounding medium and radiation field. Our goal is to explain the observed multi-wavelength emissions from the inner few parsecs of the Galaxy. We considered different scenarios: the injected particles can be either protons or electrons (or mixed) and the source may be transient or continuous.

Our analysis shows that pure hadronic injection model is not good enough to explain both X-ray and gamma-ray observations. If the hadronic model is able to reproduce the observed gamma-ray intensity, the hard X-ray flux is more than an order of magnitude lower than the observed one. We note, however, that the X-ray flux depends strongly on the density of soft photons in the region. If for some reason the density of IR photons is an order of magnitude higher than what we have estimated, the expected X-ray flux could be comparable with observations. Despite we do not know what kind of sources may increase IR photon density by an order of magnitude, such a high density could be justified if the cut-off in the TeV spectrum of the central source is indeed due to

absorption of the IR photons. Moreover, a non-negligible contribution from synchrotron emission to the hard X-rays may be expected in this case.

On the other hand, pure leptonic injection models are able to provide reasonable X-ray fluxes. Electrons are also able to reproduce gamma-ray spectrum observed by *Fermi* LAT better than hadronic models (see, e.g., Malyshev et al. 2015). Both transient and continuous models can reproduce the spatial and spectral shape of the hard X-ray emission. The only shortcoming of the continuous model is that the ionization rate in the central cavity exceeds the observed one by 4 orders of magnitude, although IR estimation of the ionization rate may not be very reliable. The problem of exceedingly high ionization rate can be resolved if we assume that the continuous source was somehow inactive for the last 100 yrs.

It is interesting to note that similar conclusion was made from X-ray observations of molecular clouds in the GC (see Inui et al. 2009; Ponti et al. 2010; Terrier et al. 2010; Nobukawa et al. 2011, and references therein). It was concluded that just about 100 years ago Sgr A* was a source of hard X-rays with a luminosity $\sim 10^{39}$ erg s^{-1}. This number almost exactly coincides with our findings. Even if this is just a coincidence, it would be interesting to find a possible connection between these phenomena.

In the mixed model that both protons and electrons are emitted by the central source, relatively low proton-to-electron ratio is necessary. The ratio of the density of proton above 1 GeV to the density of electron above 1 GeV must be smaller than 20. For comparison this proton-to-electron ratio at Earth is around $50 \sim 100$. Nevertheless, we should point out that this inferred ratio depends on ratio between gas density and soft photons density. If the density of radiation field is underestimated or if GeV particles are unable to penetrate inside the molecular cloud, then even at a higher proton-to-electron ratio the model could be tuned to reproduce the observed X-ray flux.

A.   Soft photon density in the Galactic Central Region

Our approach to calculate the density of soft photons in the Galactic center (GC) is similar to the one used by Kistler (2015). We split the overall soft photon field into four different components, each with its own temperature and spatial distribution. Explicitly, we consider UV and IR emission from the central parsec, IR emission from the circumnuclear disk (CND) and optical emission from

the Nuclear Star Cluster (NSC).

In the case of the emissions from the central parsec we adopt the data from Mezger et al. (1996). According to the paper the temperature and total luminosity of the UV emission are $T^{\mathrm{UV}} = 3 \times 10^4$ K and $L_{\mathrm{UV}} = (7.5 \pm 3.5) \times 10^7$ $L_\odot$, respectively. The corresponding average energy density of UV photons inside the central parsec is $(5.5 \pm 2.5) \times 10^4$ eV cm^{-3}. We take the lowest possible estimate and assume that the average energy density of UV photons is $w_0^{\mathrm{UV}} = 3 \times 10^4$ eV cm^{-3}. As for IR emission, we adopt $T^{\mathrm{IR}} = 170$ K and $w_0^{\mathrm{IR}} = 3.5 \times 10^3$ eV cm^{-3}.

Outside the central parsec we assume that absorption is not important and the distribution of soft photons evolve as

$$w(R) = \begin{cases} w_0 & \text{, if R} < 1 \text{ pc} \\ w_0 \left(\frac{R}{1\,\mathrm{pc}}\right)^{-2} & \text{, if R} \geq 1 \text{ pc,} \end{cases} \tag{A1}$$

where $R^2 = r^2 + z^2$.

The last two components do not have a spherically symmetric distribution and their distribution should be estimated based on the distribution of sources. If the emissivity of the sources is $\epsilon(r', z')$, the density of soft photons can be estimated as (ignore absorption)

$$w(r, z) = \frac{1}{4\pi c} \int r'\, dr' \int dz' \int \frac{\epsilon(r', z')\, d\phi'}{[(z - z')^2 + r^2 + r'^2 - 2rr'\cos\phi']}. \tag{A2}$$

In the case of IR emission from the CND, we assume that the density of sources is proportional to the density of gas described by Ferrière (2012). According to Mezger et al. (1996) and Telesco et al. (1996) the temperature of the emission is $T^{\mathrm{CND}} = 70$ K and the total luminosity is

$$L^{\mathrm{CND}} = \int 2\pi r'\, dr' \int \epsilon^{\mathrm{CND}}(r', z')\, dz' = 10^{40} \mathrm{erg\ s}^{-1}. \tag{A3}$$

In the case of the emission from the NSC we need to estimate the density of sources first. According to Schödel et al. (2014) the surface brightness of NSC can be described by a Sérsic profile

$$I(x, y) = I_{\mathrm{e}} \exp\left(-b_n \left[\left(\frac{\varrho}{R_{\mathrm{e}}}\right)^{1/n} - 1\right]\right), \quad \varrho^2 = x^2 + \frac{y^2}{q^2}, \tag{A4}$$

where ϱ is called the modified projected radius, and $q = 0.7$ is the projected minor to major axis ratio. Here x and y are the vertical and horizontal coordinates and n, b_n, R_{e} and I_{e} are fitting parameters. Their numerical values can be found in Table 3 of Schödel et al. (2014). We note that specific choice of the model from that table only slightly affects the final result.

Following Schödel et al. (2014) we assume that the distribution of sources depends only on the modified radius ρ

$$\epsilon^{\mathrm{NSC}}(r, z) = \epsilon(\rho), \quad \rho^2 = r^2 + \frac{z^2}{q_s^2}, \tag{A5}$$

where q_s is the true minor to major axis ratio. Generally speaking $q_s \neq q$. To simplify and to keep the symmetry of our model, we assume that the plane of symmetry of NSC is parallel to that of CND, i.e., inclined by 20° to the Galactic plane. The inclination makes projected minor to major axis ratio q slightly larger than the real one q_s.

Integrating the emissivity along the line-of-sight gives the surface brightness

$$I(x,y) = \frac{1}{4\pi} \int_{-\infty}^{\infty} \epsilon^{\mathrm{NSC}}(r,z)\, d\ell \,, \tag{A6}$$

where the inclination of $\theta = 20°$ is taken into account,

$$r^2 = x^2 + \ell^2 \cos^2\theta \,, \quad z = y + \ell \sin\theta \,. \tag{A7}$$

We transform Equation (A6) into discrete form and solve the resulting system of linear equations to obtain the source distribution

$$I_j = A_{i,j}\epsilon_j \,, \tag{A8}$$

where $A_{i,j}$ is the matrix produced by applying Simpson's numerical integration rule to Equation (A6). The value of q_s can be estimated: for apparent ratio $q = 0.7$ the real ratio is $q_s = 0.6$.

Knowing the source distribution $\epsilon^{\mathrm{NSC}}(r,z)$, we apply Equation(A2) to obtain the distribution of soft photons $w^{\mathrm{NSC}}(r,z)$ produced by NSC. We assume that the temperature of this emission is 3200 K.

REFERENCES

Abramowski, A., Aharonian, F., Benkhali, F. Ait et al. 2016, Nature, 531, 476

Acero, F., Ackermann, M., Ajello, M. et al. 2015, ApJS, 218, 23

Ackermann, M., Ajello, M., Atwood, W. et al. 2012, ApJ, 750, 3

Aharonian, F., Akhperjanian, A. G., Anton, G. et al. 2009, A&A, 503, 817

Archer, A., Benbow, W., Bird, R. et al. 2016, ApJ, 821, 129

Atoyan, A. M. 1992, A&A, 257, 476

Blumenthal, G. R., & Gould, R. J. 1970, Reviews of Modern Physics, 42, 237

Chernyakova, M., Malyshev, D., Aharonian, F. A. et al. 2011, ApJ, 726, 60

Chernyshov, D. O., Leung, G. C. K., Cheng, K. S., Dogiel, V. A., Tatischeff, V. 2014, arXiv:1412.2740

Christopher M. H., Scoville, N. Z., Stolovy, S. R., & Yun, Min S. 2005, ApJ, 622, 346

Dalgarno, A., Yan, M., Liu, W.-H. 1999, ApJS, 125, 237

Dogiel, V. A., Chernyshov, D. O., Tatischeff, V. et al. 2013, ApJ, 771, L43

Dogiel, V. A., Chernyshov, D. O., Kiselev, A. M., Cheng, K.-S. 2014, APh, 54, 33

Dogiel, V. A., Chernyshov, D. O., Kiselev, A. M. et al. 2015, ApJ, 809, 48

Eatough, R. P., Falcke, H., Karuppusamy, R. et al. 2013, Nature, 501, 391

Ferrière, K., Gillard, W., Jean, P. 2007, A&A, 467, 611

Ferrière, K. 2012, A&A, 540, 50

Goto, M., Indriolo, N., Geballe, T.R., Usuda, T. 2013, The Journal of Physical Chemistry A, 117, 9919

Goto, M., Geballe, T. R., Indriolo, N. et al. 2014, ApJ, 786, 96

Guo, Y., Yuan, Q., Liu, C., Li, A. 2013, JPhG, 40, 065201

Hailey, C. J., Mori, K.; Perez, K. et al. 2016, ApJ, 826, 160

Hayakawa, S. 1964, *Cosmic Ray Physics*, ed. R. E. Marshak, Interscience Monographs

Inui, T., Koyama, K., Matsumoto, H., Tsuru T. G. 2009, PASJ, 61, 241

Kamae, T., Karlsson, N., Mizuno, T., et al., 2006, ApJ, 647, 692

Killeen, N. E. B., Lo, K. Y., Crutcher, R. 1992, ApJ, 385, 58

Kistler, M. 2015, arXiv:1511.00723

Kusunose, M., & Takahara, F. 2012, ApJ, 748, 34

Linden, T., Lovegrove, E., Profumo, S. 2012, ApJ, 753, 41

Macias, O., Gordon, C., Crocker, R., Profumo, S. 2015, MNRAS, 451, 1833

Malyshev, D., Chernyakova, M., Neronov, A., Walter, R. 2015, A&A, 582, A11

Mannheim, K., & Schlickeiser, R. 1994, A&A, 286, 983

Mezger, P. G., Duschl, W. J., Zylka, R. 1996, A&ARv, 7, 289

Nobukawa, M., Ryu, S. G., Tsuru, T. G., Koyama, K. 2011, ApJL, 739, L52

Nolan, P. L., Abdo, A. A., Ackermann, M. et al. 2012, ApJS, 199, 31

Oka, T., Geballe, Th. R., Goto, M. et al. 2005, ApJ, 632, 882

Pedlar, A., Anantharamaiah, K. R., Ekers, R. D., et al. 1989, ApJ, 342, 769

Perez, K., Hailey, C. J., Bauer, F. E. 2015, Nature, 520, 646

Ponti, G., Terrier, R., Goldwurm, A. et al. 2010, ApJ, 714, 732

Tatischeff, V. 2003, *Final Stages of Stellar Evolution*, ed. C. Motch and J.-M. Hameury, EAS Publications Series (EDP Sciences: Les Ulis, France), vol. 7, pp. 79-124

Telesco, C. M., Davidson, J. A., Werner, M. W. 1996, ApJ, 456, 541

Terrier, R., Ponti, G., Belanger, G. et al. 2010, ApJ, 719, 143

Schöel, R., Feldmeier, A., Kunneriath, D. 2014, A&A, 566, A47

Strong, A. W., Porter, T. A., Digel, S. W. 2010, ApJ, 722, L58

Yusef-Zadeh, F., Roberts, D. A., Goss, W. M. et al. 1996, ApJ, 466, L25

Yusef-Zadeh, F., Arendt, R., Bushouse, H. et al. 2012, ApJ, 758, L11

Yusef-Zadeh, F., Hewitt, J. W., Wardle, M. et al. 2013, ApJ, 762, 33